RSC Advances

PAPER

View Article Online
View Journal | View Issue

Cite this: *RSC Adv.*, 2020, **10**, 29633

Quantum dot-sensitized O-linked heptazine polymer photocatalyst for the metal-free visible light hydrogen generation†

Soumadri Samanta, Sunil Kumar, V. R. Battula, Arpna Jaryal, Neha Sardana‡ and Kamalakannan Kailasam *

Received 27th April 2020
Accepted 23rd July 2020

DOI: 10.1039/d0ra03773g

rsc.li/rsc-advances

Metal-free organic polymer photocatalysts have attracted dramatic attention in the field of visible light-induced hydrogen evolution reaction (HER). Herein, we showed a polymeric O-linked heptazine polymer (OLHP) decorated with S, N co-doped graphene quantum dots (S,N-GQDs) as a photosensitizer to generate hydrogen upon quantum dot sensitization. Both of these heptazine-based systems show effective photosensitization with strong π–π interactions and enhanced photocatalytic H_2 generation (24 times) as metal-free systems. Electrochemical impedance and optical measurements show effective charge transfer kinetics with decreased charge recombination, which is responsible for the enhanced photocatalytic activity. As a result, a significant high apparent quantum yield (AQY) with highest value of 10.2% was obtained for our photocatalyst OLHP/S,N-GQD10.

Introduction

Molecular hydrogen (H_2) is considered as the most precious renewable and environment-friendly fuel due to the fact that it has high energy density and produces water as a by-product.[1–7] Visible light semiconductor-mediated photocatalytic water splitting is an inexpensive and environment friendly procedure for H_2 generation.[8–12] However, the use of expensive Pt as co-catalyst to bring down the overpotential of water splitting reaction raises the cost-related concerns for commercial applications. Thus, the search for a precious metal-free photocatalytic water splitting system for hydrogen generation is considered to be a noble mission for material science. The utilization of g-CN as a sole photocatalyst for hydrogen production has hastened the research to achieve metal-free water splitting.[13–19] However, photocatalytic systems that can extract hydrogen from water without the expense of any metal-based co-catalyst are less reported. Here, we developed a quantum dot-sensitized polymer as a hybrid system which functions as a metal-free photocatalyst for hydrogen generation.

Polymeric carbon nitrides, g-CN, commonly known as g-C_3N_4 (an N-bridged heptazine polymer) have become a research hotspot as solar-to-hydrogen producing photocatalysts.[13] During the past decade, major focus of research has been on enhancing the photo-response of the polymeric g-CN prepared mostly from the hetero atom containing alicyclic or triazine-based precursors for enhanced photocatalytic activity. Researchers have introduced structural modifications on polymeric g-CN such as metal and elemental doping,[20–23] exfoliation,[24,25] composite formation,[26–31] and organic modification as well as photosensitization of g-CN,[32,33] and reported an enhanced photocatalytic activity of the solar-to-hydrogen conversion process in the search of metal-free efficient photocatalysts. Moreover, it was also shown that the employment of heptazine-based precursors like melem and cyameluric acid proved to be viable alternatives to synthesize only heptazine containing g-CN as compared to alicyclic or triazine-based precursors that have triazine and heptazine units altogether in final structures. A typical problem that most researchers encounter is to control the formation of defective structures that arise from incomplete polymerization to get final triazine or heptazine-based polymeric g-CN materials by using the above-mentioned precursors.

In a very recent report, a photocatalyst comprised of polymeric g-CN and prepared from precursors dicyandiamide and semicarbazide hydrochloride to yield a heptazine polymer bridged through N and O atoms was reported with enhanced photocatalytic activity.[34,35] Following this work, Kailasam and group reported the synthesis of true O-linked heptazine polymer, OLHP (from cyameluric acid as a precursor) as an efficient structural variant of g-CN with enhanced photocatalytic activity

Advanced Functional Nanomaterials, Energy and Environment Unit, Institute of Nano Science and Technology (INST), Phase X, SAS Nagar, Mohali 160062, Punjab, India. E-mail: kamal@inst.ac.in

‡ Current address: Assistant Professor, Metallurgical and Materials Engineering, Room 316, Satish Dhawan Block, Indian Institute of Technology Ropar, Ropar, Punjab, India.

† Electronic supplementary information (ESI) available: XRD, EDX, FTIR, XPS, comparison of HER with 2 wt% Pt as co-catalyst, stability of H_2 evolution with 2 wt% Pt as co-catalyst, and hydrogen evolution rate for different ratios of H_2O and TEOA. See DOI: 10.1039/d0ra03773g

for hydrogen evolution.[36] It was argued that the presence of bridging O-atoms in OLHP renders better charge separation and a lifetime to charge carriers to be efficiently utilized in water reduction reaction as compared to g-CN and as a result, OLHP produces 41-fold higher H_2 compared to g-CN. However, like g-CN, OLHP required the presence of Pt-metal as a co-catalyst for water splitting. As hydrogen energy provides a major solution to the deepening environmental pollution problem, the material design strategies which lead to the enhancement in hydrogen production efficiency of known polymers/photocatalysts hold great significance. Since OLHP is a new member of the heptazine-based g-CN family, the studies exploring the increase in its photocatalytic activity are worth and warranted for arising energy needs. We anticipate that photosensitization may increase charge carrier concentration over OLHP which will be adventitious to induce the metal-free photocatalytic activity. It is to be noted that, alike g-CN so far, no reports studying the photosensitization of OLHP with quantum dots have been reported.

Generally, photosensitization has been employed to enhance the photocatalytic activity of semiconducting materials with large band gaps as photosensitization increases the photon harvesting range as well as the number of electrons on semiconductor materials.[1,37–39] The sensitizer molecules exhibit fast charge recombination property and thus lack photocatalytic H_2 generation activity. The charge recombination could be delayed if these photo-generated charge carriers from sensitizer molecules could be transferred to the low lying conduction band (CB) of a semiconductor material and thereby improving the photocatalytic property of semiconductor materials. Qin *et al.* prepared fluorescein dye-sensitized Ag/g-C_3N_4 composite photocatalysts with improved photocatalytic H_2 production under visible light irradiation.[40] Deng *et al.* prepared N-doped graphene quantum dot-sensitized Ag/g-CN with enhanced photocatalytic activity.[41] Recently, Qu *et al.* have reported S and N co-doped graphene quantum dots (S,N-GQDs) which possess smaller band gaps compared to pristine graphene sheets[42] which were used to prepare the S,N-GQDs/TiO_2 composite and showed enhanced photocatalytic activity for dye degradation application. Xie *et al.* have reported S,N-GQD-sensitized TiO_2 for visible light H_2 production.[43] It was proposed that prepared S,N-GQDs act as an electron reservoir and accelerate solid-state photo-generated electron transfer process. To add more, the S,N-GQD/g-CN composite was also reported to enhance the photocatalytic property of g-CN for dye degradation.[44] However, the potential candidature of these S,N-GQDs as a photosensitizer has not been elucidated for enhancing the photocatalytic H_2 evolution activity of organic semiconductors. Moreover, the ongoing efforts to increase the photocatalytic performances of low visible-light absorbing photocatalysts prompted us to study the effect of photosensitization on the hydrogen evolution performance of organic semiconductor materials. To the best of our knowledge, there are no reports on quantum dot-sensitized OLHP with metal-free visible light-assisted photocatalytic H_2 evolution. All these studies encouraged us to study the S,N-GQDs photosensitization effect on the photocatalytic performance of the OLHP photocatalyst.

The experimentally determined band position of S,N-GQDs elucidated that these could function as a photosensitizer for OLHP. The band position alignment of S,N-GQDs with the OLHP photocatalyst prompted us to synthesize S,N-GQDs decorated OLHP photocatalysts and study the photocatalytic activity as metal-free photocatalysts for hydrogen evolution. Thus, herein, we synthesized the sensitizer-based photocatalyst system by a one-pot hydrothermal process. The developed sensitizer-decorated photocatalyst was studied using basic characterization tools, and its optical properties were established. To our surprise, the photocatalyst exhibited water splitting activity even without the use of Pt as co-catalyst.

Experimental

Chemicals and methods

All chemicals and solvents were of analytical grade and used without further purification. Following are the chemicals and their sources of procurement: citric acid, thiourea (TCI), triethanolamine (TEOA) (Sigma Aldrich), sodium sulfate (Merck). X-ray diffraction (XRD) patterns were recorded on a Bruker D8 Advance diffractometer equipped with a scintillation counter detector with a Cu Kα radiation ($\lambda = 0.15406$ Å) source operating at 40 kV and 40 mA. DR UV-visible spectra were recorded on a Shimadzu UV-2600 spectrophotometer. SEM images were recorded on a JEOL 7600F instrument. EDX and elemental mapping were recorded using XFlash 6130 Bruker. Photoluminescence (PL) spectra were measured using a Fluorolog HORIBA instrument at an excitation wavelength of 420 nm. Fourier transformation infrared (FTIR) analysis was done by using a Bruker VERTEX70 instrument. Transmission electron microscopy analysis was done by using a JEOL 2100 instrument at an operating voltage of 200 kV. We quantified H_2 through a TCD detector using Shimadzu GC-2014. We performed the XPS analysis of our sample using the instrument PHI 5000 Versa Prob II.

Materials and sample preparation

All chemicals were of analytical grade and used without any further purification. As the physical mixing of S,N-GQDs and OLHP will result in a weak interfacial contact, a hydrothermal method was used as an optimized strategy. Firstly, OLHP-550 was prepared using the previously reported method.[36] S, N co-doped graphene quantum dots (S,N-GQDs) were synthesized following the reported method by Qu *et al.*[42] Then with as-prepared OLHP, a specific volume of S,N-GQDs was added and then sonicated for 1 h. Finally, the suspension was transferred into a teflon-lined stainless steel autoclave and kept at 100 °C for 6 h in an air oven (Fig. 1). We synthesized S,N-GQD-decorated OLHP in 4 different weight percentages (5%, 10%, 20%, and 50%). Depending on the percentage of S,N-GQDs used, the samples were named as OLHP/S,N-GQD5, OLHP/S,N-GQD10, OLHP/S,N-GQD20, and OLHP/S,N-GQD50.

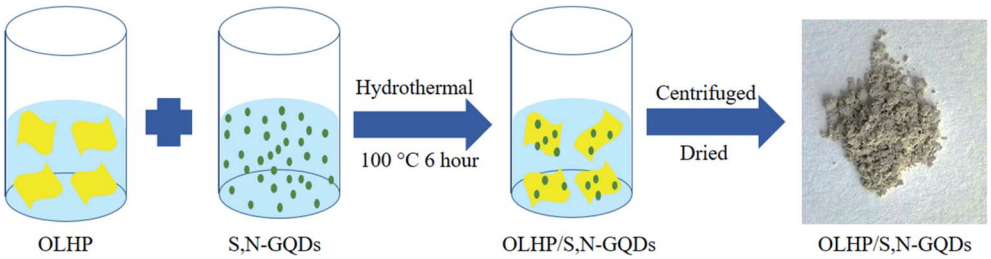

Fig. 1 Schematic illustration of S,N-GQDs decorated OLHP preparation procedure.

Photoelectrochemical measurement

Electrochemical measurements were carried out in a standard three-electrode configuration with Ag/AgCl (in saturated KCl) electrode as a reference electrode, platinum electrode as a counter electrode, and 0.2 M Na_2SO_4 aqueous solution as the electrolyte. The test results were recorded using Metrohm Autolab (M204 multichannel potentiostat galvanostat). The photocatalyst was coated on a standard glassy carbon electrode and was used as a working electrode. For the coating purpose, Nafion solution was used as a binder (2 mg photocatalyst and 20 μl of 10 wt% Nafion solution). For CV measurement, we took 0.3 mmol S,N-GQDs in 0.2 M Na_2SO_4 aqueous solution, and the standard glassy carbon electrode was used as a working electrode.

Photocatalytic H_2 evaluation reaction

Hydrogen generation by photocatalytic water splitting was carried out in a 50 ml round-bottom flask at ambient temperature and atmospheric pressure. A 400 watt Xe lamp (Oriel OPS-A100, Newport) with a 420 nm cut-off filter served as an irradiation light source to perform the photocatalytic reaction, which was positioned at a height of 10 cm from the flask. The focused intensity of the Xe lamp on the flask was about 90 mW cm^{-2}. In a typical experiment, 10 mg of the photocatalytic material was dispersed in a mixed solvent containing 27 ml DI water and 3 ml TEOA. Before each experiment, the system was first vented using a vacuum pump and then, nitrogen gas was purged for 30 min. During the reaction time, continuous stirring was done to keep the catalyst well dispersed. 2 wt% Pt as co-catalyst was deposited on the catalyst using the *in situ* photo-deposition method by directly dissolving chloroplatinic acid (H_2PtCl_6) in the reactant suspension.

Results and discussion

The TEM images of as-prepared S,N-GQDs, OLHP, and OLHP/S,N-GQD20 are shown in Fig. 2. The TEM images revealed the formation of S,N-GQDs particles with mean diameters 2.9 ± 0.59 nm (Fig. 2a and inset). A representative HRTEM image displays a lattice spacing of 2.4 Å which is similar to that of graphite (100) facets (inset to Fig. 2a).[42] Fig. 2b represents the TEM image of the S,N-GQD-modified OLHP catalyst which confirmed the presence of quantum dots over the surface of OLHP. It can be seen that S,N-GQDs agglomerate on the surface of OLHP but retain the size without affecting the lamellar morphology of the OLHP catalyst. Further, to reassure the loading of S,N-GQDs on the OLHP polymer, EDX analysis was also carried out (Table S1†). The presence of sulfur atoms indicated the decoration of S,N-GQDs which increased with an increment in the wt% of S,N-GQDs on the OLHP polymer in different samples. Elemental mapping also confirms the well-dispersion of S,N-GQDs on the surface of OLHPs (Fig. 2c–g).

The crystallographic structures of the as-synthesized OLHP/S,N-GQDs samples were revealed by powder XRD patterns (Fig. S1†). As reported earlier, OLHP exhibits an intense diffraction peak at $2\theta = 27.1°$, which has been indexed to the (002) stacked plane of conjugated heptazine units as in graphite.[36] After decorating S,N-GQDs with different proportions, no shift in the peak at $2\theta = 27.1°$ was observed, which signifies that there is no effect on the stacking arrangement of heptazine sheets in OLHP. In Fig. S1,† there is no characteristic peak for S,N-GQDs instead a broad hump can be seen which signifies that the as-prepared S,N-GQDs are quantum-sized having amorphous nature. As said, due to its amorphous nature, no significant characteristic peak appeared in S,N-GQD-decorated OLHP.

FTIR spectra (Fig. 3a) identify the surface functional groups of S,N-GQDs, OLHP, and OLHP/S,N-GQDs. For the S,N-GQDs,

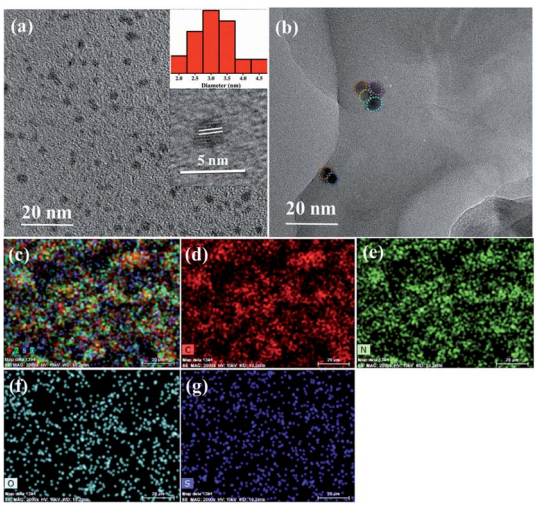

Fig. 2 (a) TEM images of S,N-GQDs (inset: particle size distribution and HRTEM of S,N-GQDs); (b) TEM image of OLHP/S,N-GQD20 and (c–g) the SEM elemental mapping of OLHP/S,N-GQD20.

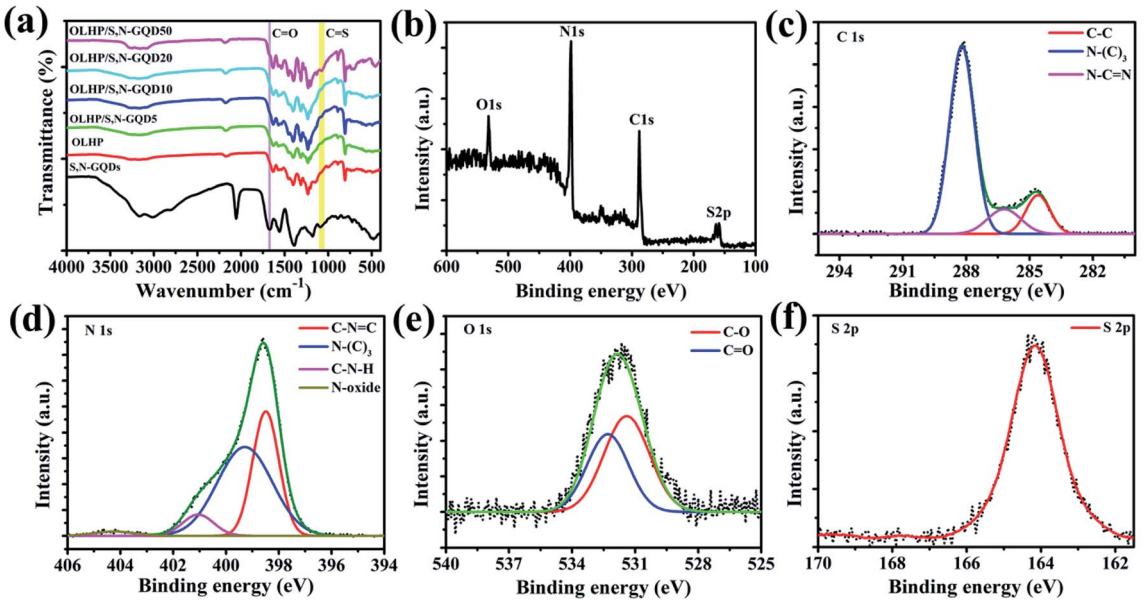

Fig. 3 (a) FTIR spectra of S,N-GQDs, OLHP and OLHP/S,N-GQDs, (b) XPS full scan, high resolution XPS of (c) C 1s, (d) N 1s, (e) O 1s and (f) S 2p of OLHP/S,N-GQD20.

the broad absorption bands in the range 3000–3500 cm^{-1} are assigned to the stretching vibrations of O–H and N–H and the absorption peaks at 1662, 1564, and 1395 cm^{-1} can be assigned to C=O, C=C, and C–N, respectively. The peak at 1084 cm^{-1} in S,N-GQDs is attributed to the C=S group.[42] OLHP shows absorption peaks which correspond to the functional groups of the tri-*s*-triazine structure (804 cm^{-1}), heptazine heterocycles (1633–1236 cm^{-1}), and ternary hydroxyl group (3000–3400 cm^{-1}).[36] The OLHP/S,N-GQDs exhibit an FTIR spectrum with characteristics peaks of both OLHP and S,N-GQDs. The presence of C=S stretching in OLHP/S,N-GQDs confirms the decoration of S,N-GQDs on OLHP. X-ray photoelectron spectroscopy (XPS) was also employed to identify the composition of OLHP/S,N-GQD20. The full scan XPS spectrum is shown in Fig. 3b, where 4 peaks were observed with the binding energy (BE) values of 531.8, 398.6, 288.6, and 164.2 eV, which correspond to O 1s, N 1s, C 1s, and S 2p, respectively.[45–48] High-resolution spectra of C 1s can be fitted into three peaks at BE of 284.5, 286.6, and 288.2 eV (Fig. 3c). Two weak peaks at the BE of 284.5 and 286.6 eV were ascribed to adventitious carbon C–C and N–$(C)_3$ bonds, respectively. The main peak at a BE of 288.2 eV was assigned to sp^2 C atoms bonded to nitrogen, C–N=C bond in the heptazine ring. Fig. 3d shows the high-resolution spectra of N 1s. The deconvolution of N 1s gives four peaks at 398.5, 399.4, 400.9, and 404.3 eV, which corresponds to C–N=C, N–$(C)_3$, C–N–H, and N–oxides bonds. As shown in Fig. 3e, the deconvolution of O 1s renders two peaks at 531.4 and 532.3 eV, which corresponds to C=O (oxygen doubly bonded to aromatic carbon) and C–O (oxygen singly bonded to aliphatic carbon) bonds, *i.e.*, C–OH groups, respectively.[47] The high-resolution XPS spectra (Fig. 3f) of S 2p of OLHP/S,N-GQD20 clearly shows a peak at 164.2 eV, which corresponds to S 2p of the sulfur atom (thiophene) present on the surface of OLHP/S,N-GQD20 (Table S2†).

Furthermore, the effect on the optical properties of S,N-GQD-modified OLHP was assessed by using UV-vis spectroscopy (Fig. 4a). Individually, OLHP exhibits its characteristic absorption band edge at around 445 nm, while S,N-GQDs showed two characteristic strong absorption bands at 440 and 595 nm. It was found that OLHP/S,N-GQDs exhibited a blue shift in the band-edge absorption of OLHP photocatalyst, and an additional tailing in the visible region was observed. Though the band-edge absorption peak at 595 nm is not visible, an absorbance tailing due to S,N-GQDs is observed. This might be responsible for a broad shoulder peak observed at 700 nm for OLHP/S,N-GQDs. Moreover, the blue shift in absorption onset and absorption tailing suggested the interfacial interaction between OLHP and S,N-GQDs. The charge transfer and recombination characteristics of photo-generated electron–hole pairs of all the catalysts were compared by performing photoluminescence (PL) studies (Fig. 4b). The PL spectrum of OLHP shows maximum peak intensity at 460 nm ($\lambda_{exc} = 420$ nm), whereas the S,N-GQD-decorated OLHP has an intense peak at 468 nm. Lower intensity PL emission of the S,N-GQD-decorated OLHP signifies reduced recombination rate, which indicates that S,N-GQDs form well interfacial contact with OLHP causing enhanced electron–hole separation. As a result, photocatalytic activity is improved significantly.

The possible band position of S,N-GQDs was measured by carrying out cyclic voltammetric (CV) measurement (Fig. 5a). From CV, the HOMO level was calculated from the first oxidation onset.[49] The oxidation onset was assessed at 0.39 V. The absence of a reduction peak in the used potential window prompted us to calculate LUMO using the optical band gap of S,N-GQDs. The optical band gap was calculated to be 1.91 eV

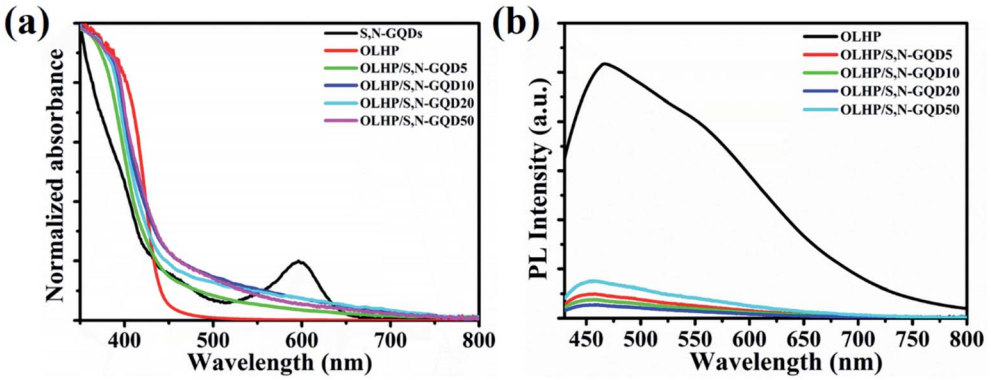

Fig. 4 (a) UV-vis spectra of S,N-GQDs, OLHP and OLHP/S,N-GQDs and (b) PL spectra of S,N-GQDs, OLHP and OLHP/S,N-GQDs.

from the UV-vis spectra of S,N-GQDs (corresponding absorption band edge at 648 nm) (Fig. 4a). Thus, the LUMO level could be assessed at 0.39 V (*vs.* Ag/AgCl), which provided the HOMO level at −1.52 V (*vs.* Ag/AgCl). The conduction band minima (CBM) and valence band maxima (VBM) for OLHP lie at −1.32 V (*vs.* Ag/AgCl) and 1.35 V (*vs.* Ag/AgCl), respectively, with an optical band gap of 2.67 eV.[36] The corresponding band positions for both the photosensitizer and photocatalyst (with respect to NHE) are shown in Fig. 5b, which clearly satisfies the requirement for the possible feasibility of electron transfer through the dye sensitization process as the CBM of S,N-GQDs lies just more negative to the CBM of OLHP.[36,50] This band arrangement favors more electron injection onto the photocatalyst, which may enhance the photocatalytic activity of OLHP for possible hydrogen generation.

To reaffirm our band positions, we carried out the valance band X-ray photoelectron spectroscopy (XPS) of OLHP/S,N-GQD20 (Fig. 6b). As shown in Fig. 6a, the valance band maxima (VBM) of OLHP/S,N-GQD20 was measured at about 1.23 eV and combing the measured optical band gap (2.5 eV) of OLHP/S,N-GQD20 (Fig. 6a), the conduction band minima (CBM) was located at −1.27 eV. According to these results, OLHP/S,N-GQD20 has a potential to achieve hydrogen evolution through water splitting. The observed band structure of OLHP/S,N-GQD20 is believed to be tuned according to the band positions of its precursors (OLHP and S,N-GQDs).

Further, the photocatalytic performance of S,N-GQD-decorated OLHP was investigated for H_2 evolution through water splitting under visible light (>420 nm) for 4 h with triethanolamine (TEOA) as a sacrificial reagent. Though OLHP and S,N-GQDs didn't produce any H_2 in the absence of Pt as co-catalyst, but the OLHP/S,N-GQDs generated hydrogen without the use of Pt as co-catalyst (Fig. 7). Further, the photocatalytic H_2 evolution experiments were also carried for the photocatalyst with different wt% of S,N-GQDs loaded on the photocatalyst. It was found that all S,N-GQD-modified OLHP photocatalysts produced hydrogen efficiently compared to OLHP in metal-free conditions (as shown in Fig. 7). It was also observed that with the increase in the wt% of S,N-GQDs in OLHP from 5–20 wt%, production of H_2 increased from 13.6 to 23.9 μmol h^{-1} g^{-1}. Further, the increasing amount of S,N-GQDs (50 wt%), resulted in a decrement in H_2 evolution.

We interpret that, as the photocatalytic activity of OLHP is enhanced by the strong absorption ability of S,N-GQDs in far visible region combined with the synergistic effect of both the systems for favorable metal-free H_2 evolution. As S,N-GQDs and OLHP are structurally similar having strong π–π interaction between the heptazine units, they result in effective interfacial heterostructure formation. It is also clear from the band diagram (Fig. 5b) that S,N-GQDs can inject the photogenerated electrons into the CBM of OLHP, which will populate the conduction band of OLHP utilized for the reduction of protons

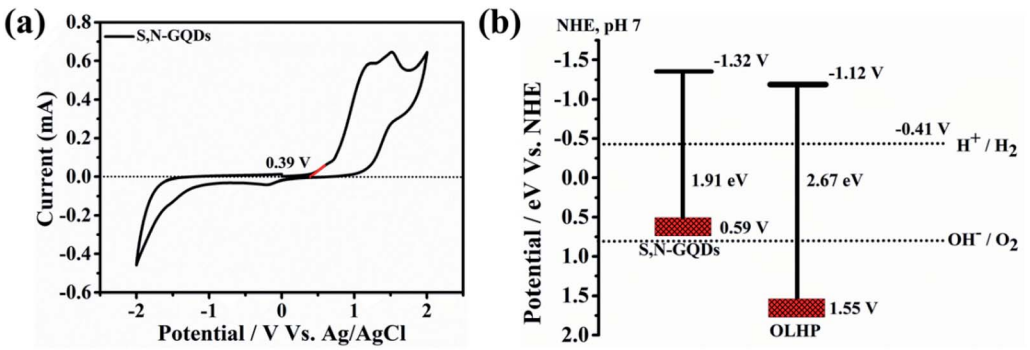

Fig. 5 (a) Voltammogram of S,N-GQDs, (b) band energy diagram of S,N-GQDs and OLHP.

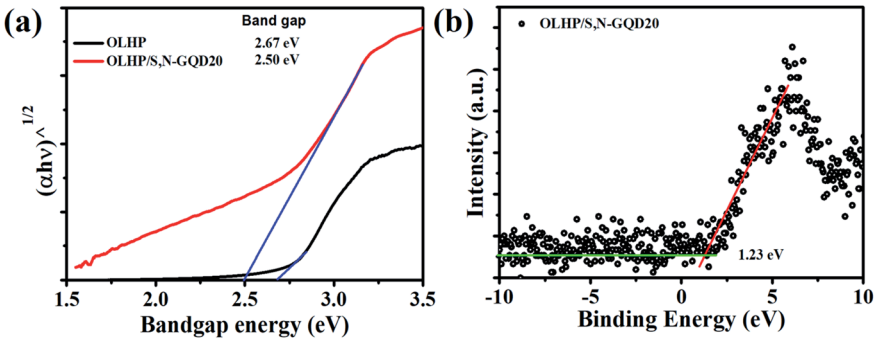

Fig. 6 (a) Tauc plot of OLHP and OLHP/S,N-GQD20 (b) valance band XPS of OLHP/S,N-GQD20.

to hydrogen over OLHP surface. So, it was observed that with an increase in the wt% of S,N-GQDs in OLHP from 5–20 wt%, the production of H_2 increased. But a further increasing amount of S,N-GQDs (50 wt%) causes enlargement and aggregation of S,N-GQDs on the surface of OLHP, thus S,N-GQDs loses its activity as a photosensitizer. Accordingly, this results in the decrement of photocatalytic activity and H_2 evolution.

We anticipated to use Pt (2 wt% Pt) as a metal co-catalyst to OLHP/S,N-GQDs for performing the photocatalytic H_2 evolution activity (Fig. S2†). The H_2 production increased from OLHP/S,N-GQD5 (138.3 μmol g^{-1} h^{-1}) to OLHP/S,N-GQD10 (167.8 μmol g^{-1} h^{-1}). The higher H_2 evolution for OLHP/S,N-GQD10 is 2.11 times more than that observed for OLHP (79.46 μmol g^{-1} h^{-1}) under similar conditions. Thus, it is understandable that when Pt is used as co-catalyst, the electrons from the photosensitized CBM of photocatalyst are easily transferred to Pt, and its high electron conductivity and lower over potential reduce the H_2O molecules to generate H_2 more efficiently. However, for OLHP/S,N-GQD20 and OLHP/S,N-GQD50, we observed lower H_2 production rates with 137.4 and 90.0 μmol g^{-1} h^{-1}, respectively.

We have calculated the apparent quantum yield (AQY) for our best photocatalyst under similar conditions without any co-catalyst and with 2 wt% Pt as co-catalyst. The values of apparent quantum yield depend on measurement methods, reaction conditions, *etc.* In this experiment, 400 nm band pass filter was used and the incident light intensity was measured with the help of a Ray virtual radiation actinometer (Newport, Model: 91150V). The apparent quantum efficiency of H_2 evolution was calculated using the formula,

$$\text{AQY } (\%) = \frac{\text{number of } H_2 \text{ molecules evolved} \times 2}{\text{number of incident photons}} \times 100\%$$

We got 10.2% AQY for the OLHP/S,N-GQD10 sample with 2 wt% platinum as co-catalyst. We have quantified AQY for OLHP/S,N-GQD20 without using any co-catalyst and got 1.3% AQY.

To ensure the catalytic charge transfer kinetics, electrochemical impedance spectroscopy (EIS) measurements were performed. Fig. 8 shows the Nyquist plot for OLHP and OLHP/S,N-GQD20. It was observed that the arc radius of OLHP/S,N-GQD20 is smaller than OLHP. Generally, smaller arc radius represents higher facial charge transfer across the catalyst and electrolyte.[46–51] Hence the decrease in arc radius indicates more facile transfer of charges on the catalyst interface of S,N-GQDs and OLHP. Incidentally, UV-vis, PL, and EIS measurements clearly reveal the role of the S,N-GQD-sensitized OLHP samples. Thus, S,N-GQDs help causing absorption in wide visible spectrum, reducing charge recombination, and accelerating reaction kinetics and suitable band alignment, which improved the visible light-assisted photocatalytic H_2 evolution.

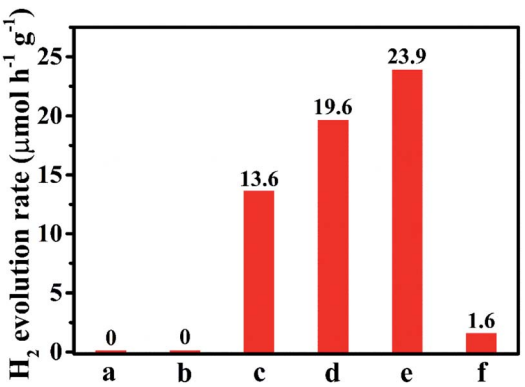

Fig. 7 Comparison of HER of (a) OLHP, (b) S,N-GQDs, (c) OLHP/S,N-GQD5, (d) OLHP/S,N-GQD10 (e) OLHP/S,N-GQD20 and (f) OLHP/S,N-GQD50.

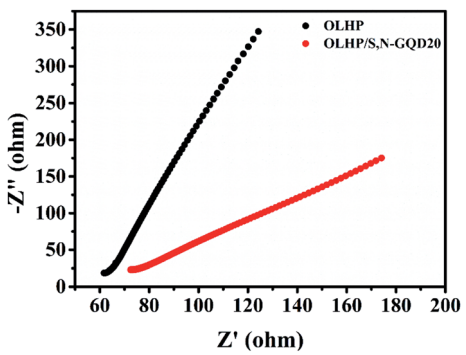

Fig. 8 EIS Nyquist plot for OLHP and OLHP/S,N-GQD20.

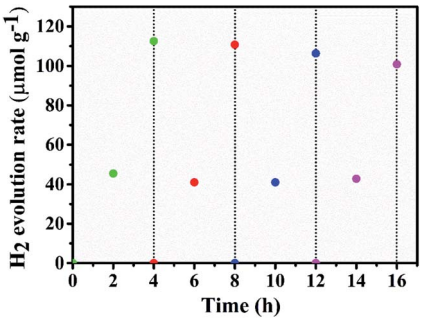

Fig. 9 Stability cycle of H_2 evolution of OLHP/S,N-GQD20.

Further, in order to check the stability and robustness of the photocatalyst, H_2 evolution was monitored for 16 h in the absence of co-catalyst without any further addition of TEOA (Fig. 9). After every 4 h, the reaction vessel was evacuated and purged with N_2. The photocatalytic activity of OLHP/S,N-GQD20 showed constant H_2 evolution even after 16 h with a slight decline in the activity which may be due to the decrease in concentration of hole scavenger (TEOA). The stability of H_2 evolution of the photocatalyst in the presence of 2 wt% Pt as co-catalyst is also studied under the same conditions stated above. The photocatalytic H_2 evolution of OLHP/S,N-GQD10 showed constant rate even after 16 h with a slight decline in the activity, which may be due to the decrease in TEOA concentration (Fig. S3†).

Decorated S,N-GQDs on the surface of OLHP work as a mediated route for electron passage from excited S,N-GQDs to the conduction band (CB) of photocatalyst and then to Pt particles. As Pt has low activation energy, it acts as a rich hydrogen active site where the electrons split water to produce H_2 under visible light irradiation. The plausible mechanism of hydrogen evolution from the aqueous TEOA solution using OLHP/S,N-GQDs under visible light ($\lambda > 420$ nm) irradiation is given as follows:

$$\text{OLHP/S,N-GQD} \rightarrow \text{OLHP}(h_{VB}^{+} + e_{CB}^{-})\text{/S,N-GQD}^{+} + e^{-}$$

$$\text{OLHP}(h_{VB}^{+} + e_{CB}^{-})\text{/S,N-GQD}^{+} + e^{-} \rightarrow \text{OLHP}(h_{VB}^{+} + e_{CB}^{-} + e^{-})\text{/S,N-GQD}^{+}$$

$$\text{OLHP}(h_{VB}^{+} + e_{CB}^{-} + e^{-})\text{/S,N-GQD}^{+} + 2\text{TEOA} \rightarrow \text{OLHP}(e_{CB}^{-} + e^{-})\text{/S,N-GQD} + 2\text{TEOA}^{+}$$

$$\text{OLHP}(e_{CB}^{-} + e^{-})\text{/S,N-GQD} \rightarrow \text{OLHP/S,N-GQD} + 2e^{-}$$

$$2e^{-} + 2H_2O \rightarrow H_2 + 2OH^{-}$$

Conclusions

A series of OLHP/S,N-GQDs photocatalysts were prepared by a hydrothermal method. The band positions were determined by UV-vis and Mott–Schottky analyses. Electrochemical and optical measurements showed the photosensitizing ability, facile transfer of charge carriers on the interface along with the wide absorbance range in the visible region. The as-prepared photocatalyst shows metal-free visible light-assisted photocatalytic water splitting for H_2 evolution which is about 23.9 μmol g^{-1} h^{-1}. Thus, this present work may open new avenues to study the role and effect of other quantum dots as photosensitizers for H_2 production in metal-free conditions. Furthermore, in the presence of Pt as co-catalyst, H_2 evolution becomes 2.11 times higher (167.8 μmol g^{-1} h^{-1}) than that of pristine OLHP with the AQY of 10.2%. We presume that this study establishes the role of S,N-GQDs as an efficient photosensitizer in the field of energy conversion.

Conflicts of interest

Authors declare no competing financial interests.

Acknowledgements

Soumadri Samanta thank INST Mohali for financial support. Dr K. Kailasam thanks Department of Science and Technology, India (DST) for the DST-Nano Mission NATDP funded Technology Project, File No. SR/NM/NT-06/2016.

References

1 Y. H. Jang, K. Chung, L. N. Quan, B. Špačková, H. Šípová, S. Moon, W. J. Cho, H.-Y. Shin, Y. J. Jang, J.-E. Lee, S. T. Kochuveedu, M. J. Yoon, J. Kim, S. Yoon, J. K. Kim, D. Kim, J. Homola and D. H. Kim, Configuration-controlled Au nanocluster arrays on inverse micelle nanopatterns: versatile platforms for SERS and SPR sensors, *Nanoscale*, 2013, **5**(24), 12261–12271.

2 D. Popugaeva, T. Tian and A. K. Ray, Hydrogen production from aqueous triethanolamine solution using Eosin Y-sensitized ZnO photocatalyst doped with platinum, *Int. J. Hydrogen Energy*, 2020, **45**(19), 11097–11107.

3 X. Chen, S. Shen, L. Guo and S. S. Mao, Semiconductor-based Photocatalytic Hydrogen Generation, *Chem. Rev.*, 2010, **110**(11), 6503–6570.

4 P. Deng, M. Gan, X. Zhang, Z. Li and Y. Hou, Non-noble-metal Ni nanoparticles modified N-doped g-C_3N_4 for efficient photocatalytic hydrogen evolution, *Int. J. Hydrogen Energy*, 2019, **44**(5), 2675–2684.

5 Y. B. Li, T. Li, X. C. Dai, M. H. Huang, Y. He, G. Xiao and F. X. Xiao, Cascade Charge Transfer Mediated by *In-situ* Interface Modulation Toward Solar Hydrogen Production, *J. Mater. Chem. A*, 2019, **7**(15), 8938–8951.

6 L. R. Nagappagari, S. Samanta, N. Sharma, V. R. Battula and K. Kailasam, Synergistic Effect of Noble Metal free $Ni(OH)_2$ co-catalyst and Ternary $ZnIn_2S_4$/g-C_3N_4 Heterojunction for Enhanced Visible Light Photocatalytic Hydrogen Evolution, *Sustainable Energy Fuels*, 2020, **4**(2), 750–759.

7 C. Bai, J. Bi, J. Wu, Y. Xu, S. Wohlrab, Y. Han and X. Zhang, *In situ* solid-phase fabrication of Ag/AgX (X=Cl, Br, I)/g-C_3N_4 composites for enhanced visible-light hydrogen evolution, *Int. J. Hydrogen Energy*, 2019, **44**(39), 21397–21405.

8 K. Maeda, K. Teramura, D. Lu, T. Takata, N. Saito, Y. Inoue and K. Domen, Photocatalyst releasing hydrogen from water, *Nature*, 2006, **440**, 295.

9 W.-J. Ong, L.-L. Tan, Y. H. Ng, S.-T. Yong and S.-P. Chai, Graphitic Carbon Nitride ($g\text{-}C_3N_4$)-Based Photocatalysts for Artificial Photosynthesis and Environmental Remediation: Are We a Step Closer To Achieving Sustainability?, *Chem. Rev.*, 2016, **116**(12), 7159–7329.

10 Q. Yang, Z. Li, C. C. Chen, Z. Zhang and X. Fang, Enhanced charge separation and transport efficiency induced by vertical slices on the surface of carbon nitride for visible-light-driven hydrogen evolution, *RSC Adv.*, 2019, **9**(8), 4404–4414.

11 H. Li, Y. Xia, Z. Liang, G. Ba and H. Hou, Energy Band Engineering of Polymeric Carbon Nitride with Indium Doping for High Enhancement in Charge Separation and Photocatalytic Performance, *ACS Appl. Energy Mater.*, 2020, **3**(1), 377–386.

12 T. Ahmed, M. Ammar, A. Saleem, H. L. Zhang and H. B. Xu, Z-scheme 2D-m-$BiVO_4$ networks decorated by a g-CN nanosheet heterostructured photocatalyst with an excellent response to visible light, *RSC Adv.*, 2020, **10**(6), 3192–3202.

13 X. Wang, K. Maeda, A. Thomas, K. Takanabe, G. Xin, J. M. Carlsson, K. Domen and M. Antonietti, A metal-free polymeric photocatalyst for hydrogen production from water under visible light, *Nat. Mater.*, 2008, **8**, 76.

14 L. Lin, H. Ou, Y. Zhang and X. Wang, Tri-s-triazine-Based Crystalline Graphitic Carbon Nitrides for Highly Efficient Hydrogen Evolution Photocatalysis, *ACS Catal.*, 2016, **6**(6), 3921–3931.

15 H. Dou, S. Zheng and Y. Zhang, The effect of metallic Fe(II) and nonmetallic S co-doping on the photocatalytic performance of graphitic carbon nitride, *RSC Adv.*, 2018, **8**(14), 7558–7568.

16 D. Peng, H. Wang, K. Yu, Y. Chang, X. Ma and S. Dong, Photochemical preparation of the ternary composite CdS/Au/$g\text{-}C_3N_4$ with enhanced visible light photocatalytic performance and its microstructure, *RSC Adv.*, 2016, **6**(81), 77760–77767.

17 A. Thomas, A. Fischer, F. Goettmann, M. Antonietti, J.-O. Müller, R. Schlögl and J. M. Carlsson, Graphitic carbon nitride materials: variation of structure and morphology and their use as metal-free catalysts, *J. Mater. Chem.*, 2008, **18**(41), 4893–4908.

18 M. Aleksandrzak, K. Sielicki and E. Mijowska, Enhancement of photocatalytic hydrogen evolution with catalysts based on carbonized MOF5 and $g\text{-}C_3N_4$, *RSC Adv.*, 2020, **10**(7), 4032–4039.

19 H. Xu, J. Yi, X. She, Q. Liu, L. Song, S. Chen, Y. Yang, Y. Song, R. Vajtai, J. Lou, H. Li, S. Yuan, J. Wu and P. M. Ajayan, 2D heterostructure comprised of metallic 1T-MoS_2/Monolayer O-$g\text{-}C_3N_4$ towards efficient photocatalytic hydrogen evolution, *Appl. Catal., B*, 2018, **220**, 379–385.

20 J. Ran, T. Y. Ma, G. Gao, X.-W. Du and S. Z. Qiao, Porous P-doped graphitic carbon nitride nanosheets for synergistically enhanced visible-light photocatalytic H_2 production, *Energy Environ. Sci.*, 2015, **8**(12), 3708–3717.

21 Y. Yang, J. Liu, C. Zhou, P. Zhang, S. Guo, S. Li, X. Meng, Y. Lu, H. Xu, H. Ma and L. Chen, In situ self-assembly synthesis of carbon self-doped graphite carbon nitride hexagonal tubes with enhanced photocatalytic hydrogen e*volution*, *Int. J. Hydrogen Energy*, 2019, **44**(50), 27354–27362.

22 M. Zhang, Z. Liu, Y. Gao and L. Shu, Ag modified $g\text{-}C_3N_4$ composite entrapped PES UF membrane with visible-light-driven photocatalytic antifouling performance, *RSC Adv.*, 2017, **7**(68), 42919–42928.

23 S. Sun, J. Li, J. Cui, X. Gou, Q. Yang, Y. Jiang, S. Liang and Z. Yang, Simultaneously engineering K-doping and exfoliation into graphitic carbon nitride ($g\text{-}C_3N_4$) for enhanced photocatalytic hydrogen production, *Int. J. Hydrogen Energy*, 2019, **44**(2), 778–787.

24 Q. Liu, J. Shen, X. Yu, X. Yang, W. Liu, J. Yang, H. Tang, H. Xu, H. Li, Y. Li and J. Xu, Unveiling the origin of boosted photocatalytic hydrogen evolution in simultaneously (S, P, O)-Codoped and exfoliated ultrathin $g\text{-}C_3N_4$ nanosheets, *Appl. Catal., B*, 2019, **248**, 84–94.

25 Y.-P. Zhu, T.-Z. Ren and Z.-Y. Yuan, Mesoporous Phosphorus-Doped $g\text{-}C_3N_4$ Nanostructured Flowers with Superior Photocatalytic Hydrogen Evolution Performance, *ACS Appl. Mater. Interfaces*, 2015, **7**(30), 16850–16856.

26 X. Wei, C. Shao, X. Li, N. Lu, K. Wang, Z. Zhang and Y. Liu, Facile *in situ* synthesis of plasmonic nanoparticles-decorated $g\text{-}C_3N_4/TiO_2$ heterojunction nanofibers and comparison study of their photosynergistic effects for efficient photocatalytic H_2 evolution, *Nanoscale*, 2016, **8**(21), 11034–11043.

27 Y. Xu, C. Du, C. Zhou and S. Yang, Ternary noble-metal-free heterostructured NiS-CuS-C_3N_4 with near-infrared response for enhanced photocatalytic hydrogen evolution, *Int. J. Hydrogen Energy*, 2020, **45**(7), 4084–4094.

28 F. He, G. Chen, Y. Yu, S. Hao, Y. Zhou and Y. Zheng, Facile Approach to Synthesize g-PAN/$g\text{-}C_3N_4$ Composites with Enhanced Photocatalytic H2 Evolution Activity, *ACS Appl. Mater. Interfaces*, 2014, **6**(10), 7171–7179.

29 H. Yan and H. Yang, TiO2–$g\text{-}C_3N_4$ composite materials for photocatalytic H_2 evolution under visible light irradiation, *J. Alloys Compd.*, 2011, **509**(4), 26–29.

30 Q. Liu, T. Chen, Y. Guo, Z. Zhang and X. Fang, Ultrathin $g\text{-}C_3N_4$ nanosheets coupled with carbon nanodots as 2D/0D composites for efficient photocatalytic H_2 evolution, *Appl. Catal., B*, 2016, **193**, 248–258.

31 D. Zeng, P. Wu, W.-J. Ong, B. Tang, M. Wu, H. Zheng, Y. Chen and D.-L. Peng, Construction of network-like and flower-like 2H-$MoSe_2$ nanostructures coupled with porous $g\text{-}C_3N_4$ for noble-metal-free photocatalytic H_2 evolution under visible light, *Appl. Catal., B*, 2018, **233**, 26–34.

32 X. Zhang, T. Peng, L. Yu, R. Li, Q. Li and Z. Li, Visible/Near-Infrared-Light-Induced H2 Production over $g\text{-}C_3N_4$ Co-sensitized by Organic Dye and Zinc Phthalocyanine Derivative, *ACS Catal.*, 2015, **5**(2), 504–510.

33 X. Wang, J. Cheng, H. Yu and J. Yu, A facile hydrothermal synthesis of carbon dots modified $g\text{-}C_3N_4$ for enhanced photocatalytic H_2-evolution performance, *Dalton Trans.*, 2017, **46**(19), 6417–6424.

34 F. Wei, Y. Liu, H. Zhao, X. Ren, J. Liu, T. Hasan, L. Chen, Y. Li and B.-L. Su, Oxygen self-doped g-C_3N_4 with tunable electronic band structure for unprecedentedly enhanced photocatalytic performance, *Nanoscale*, 2018, **10**(9), 4515–4522.

35 Y. Wang, M. K. Bayazit, S. J. A. Moniz, Q. Ruan, C. C. Lau, N. Martsinovich and J. Tang, Linker-controlled polymeric photocatalyst for highly efficient hydrogen evolution from water, *Energy Environ. Sci.*, 2017, **10**(7), 1643–1651.

36 V. R. Battula, S. Kumar, D. K. Chauhan, S. Samanta and K. Kailasam, A true oxygen-linked heptazine based polymer for efficient hydrogen evolution, *Appl. Catal., B*, 2019, **244**, 313–319.

37 W. J. Youngblood, S.-H. A. Lee, K. Maeda and T. E. Mallouk, Visible Light Water Splitting Using Dye-Sensitized Oxide Semiconductors, *Acc. Chem. Res.*, 2009, **42**(12), 1966–1973.

38 Y.-S. Chen and P. V. Kamat, Glutathione-Capped Gold Nanoclusters as Photosensitizers. Visible Light-Induced Hydrogen Generation in Neutral Water, *J. Am. Chem. Soc.*, 2014, **136**(16), 6075–6082.

39 R. Abe, K. Shinmei, N. Koumura, K. Hara and B. Ohtani, Visible-Light-Induced Water Splitting Based on Two-Step Photoexcitation between Dye-Sensitized Layered Niobate and Tungsten Oxide Photocatalysts in the Presence of a Triiodide/Iodide Shuttle Redox Mediator, *J. Am. Chem. Soc.*, 2013, **135**(45), 16872–16884.

40 J. Qin, J. Huo, P. Zhang, J. Zeng, T. Wang and H. Zeng, Improving the photocatalytic hydrogen production of Ag/g-C_3N_4 nanocomposites by dye-sensitization under visible light irradiation, *Nanoscale*, 2016, **8**(4), 2249–2259.

41 Y. Deng, L. Tang, C. Feng, G. Zeng, J. Wang, Y. Lu, Y. Liu, J. Yu, S. Chen and Y. Zhou, Construction of Plasmonic Ag and Nitrogen-Doped Graphene Quantum Dots Codecorated Ultrathin Graphitic Carbon Nitride Nanosheet Composites with Enhanced Photocatalytic Activity: Full-Spectrum Response Ability and Mechanism Insight, *ACS Appl. Mater. Interfaces*, 2017, **9**(49), 42816–42828.

42 D. Qu, M. Zheng, P. Du, Y. Zhou, L. Zhang, D. Li, H. Tan, Z. Zhao, Z. Xie and Z. Sun, Highly luminescent S, N co-doped graphene quantum dots with broad visible absorption bands for visible light photocatalysts, *Nanoscale*, 2013, **5**(24), 12272–12277.

43 H. Xie, C. Hou, H. Wang, Q. Zhang and Y. S. Li, N Co-Doped Graphene Quantum Dot/TiO_2 Composites for Efficient Photocatalytic Hydrogen Generation, *Nanoscale Res. Lett.*, 2017, **12**(1), 400.

44 A. Cai, Q. Wang, Y. Chang and X. Wang, Graphitic carbon nitride decorated with S,N co-doped graphene quantum dots for enhanced visible-light-driven photocatalysis, *J. Alloys Compd.*, 2017, **692**, 183–189.

45 C. Rajkumar, P. Veerakumar, S. M. Chen, B. Thirumalraj and K. C. Lin, Ultrathin Sulfur-Doped Graphitic Carbon Nitride Nanosheets As Metal-Free Catalyst for Electrochemical Sensing and Catalytic Removal of 4-Nitrophenol, *ACS Sustainable Chem. Eng.*, 2018, **6**(12), 16021–16031.

46 Q. Xu, C. Jiang, B. Cheng and J. Yu, Enhanced visible-light photocatalytic H2-generation activity of carbon/g-C_3N_4 nanocomposites prepared by two-step thermal treatment, *Dalton Trans.*, 2017, **46**(32), 10611–10619.

47 A. Ganguly, S. Sharma, P. Papakonstantinou and J. Hamilton, Probing the Thermal Deoxygenation of Graphene Oxide Using High-Resolution *In Situ* X-ray-Based Spectroscopies, *J. Phys. Chem. C*, 2011, **115**, 17009–17019.

48 S. Rasalingam, H. S. Kibombo, C. M. Wu, S. Budhi, R. Peng, J. Baltrusaitis and R. T. Koodali, Influence of Ti–O–Si hetero-linkages in the photocatalytic degradation of Rhodamine B, *Catal. Commun.*, 2013, **31**, 66–70.

49 C. M. Cardona, W. Li, A. E. Kaifer, D. Stockdale and G. C. Bazan, Electrochemical Considerations for Determining Absolute Frontier Orbital Energy Levels of Conjugated Polymers for Solar Cell. Applications, *Adv. Mater.*, 2011, **23**(20), 2367–2371.

50 P. Chowdhury, G. Malekshoar and A. K. Ray, Dye-Sensitized Photocatalytic Water Splitting and Sacrificial Hydrogen Generation: Current Status and Future Prospects, *Inorganics*, 2017, **5**(2), 34.

51 X. Wang, J. Cheng, H. Yu and J. Yu, A facile hydrothermal synthesis of carbon dotsmodified g-C_3N_4 for enhanced photocatalytic H $_2$-evolution performance, *Dalton Trans.*, 2017, **46**(19), 6417–6424.